

## Noncoplanar antiferromagnetism induced zero thermal expansion behavior in the antiperovskite $\text{Mn}_3\text{Sn}_{0.5}\text{Zn}_{0.5}\text{C}_x$

Zhijie Ma <sup>1,2</sup> Ying Sun <sup>1,\*</sup> Huiqing Lu,<sup>3</sup> Kewen Shi,<sup>2</sup> Sihao Deng,<sup>4</sup> Xiuliang Yuan,<sup>1</sup> Weichang Hao <sup>1</sup> Yi Du <sup>1</sup>  
Yuanhua Xia,<sup>5</sup> Leiming Fang <sup>5</sup> Jinbo Yang <sup>6</sup> Wenyun Yang,<sup>6</sup> Claire V. Colin <sup>7</sup> Huaiming Guo,<sup>1</sup>  
Xiaobai Ma <sup>8</sup> Dongfeng Chen,<sup>8</sup> and Cong Wang<sup>1,2,†</sup>

<sup>1</sup>*School of Physics, Beihang University, Beijing 100191, China*

<sup>2</sup>*School of Integrated Circuit Science and Engineering, Beihang University, Beijing 100191, China*

<sup>3</sup>*Key Laboratory for Photonic and Electronic Bandgap Materials, Ministry of Education, School of Physics and Electronic Engineering, Harbin Normal University, Harbin 150025, China*

<sup>4</sup>*Spallation Neutron Source Science Center, Dongguan 523803, China*

<sup>5</sup>*Key Laboratory of Neutron Physics and Institute of Nuclear Physics and Chemistry, China Academy of Engineering Physics, Mianyang 621999, China*

<sup>6</sup>*State Key Laboratory for Mesoscopic Physics, School of Physics, Peking University, Beijing 100871, China*

<sup>7</sup>*Institut NEEL, Université Grenoble Alpes, CNRS, F-38000 Grenoble, France*

<sup>8</sup>*Department of Nuclear Physics, China Institute of Atomic Energy, Beijing 102413, China*



(Received 14 February 2022; revised 18 October 2022; accepted 16 February 2023; published 14 March 2023)

Zero thermal expansion (ZTE) is one of the most fascinating phenomena in condensed-matter physics due to its strong correlation essence and great application prospect. However, the origin of ZTE remains elusive and it becomes an overwhelming challenge to realize the controllable design for which magnetic interaction plays a key role. In this work, with the help of neutron powder diffraction analysis, a noncoplanar  $[\frac{1}{2}, \frac{1}{2}, \frac{1}{2}]$  antiferromagnetic (AFM) phase is experimentally obtained in the antiperovskite system  $\text{Mn}_3\text{Sn}_{0.5}\text{Zn}_{0.5}\text{C}_x$ . It shows ZTE behavior in a particularly wide temperature range from 10 to 162 K with linear thermal expansion coefficient  $9.3 \times 10^{-7} \text{ K}^{-1}$ . Herein, the theoretical spin model is combined with the experimental results to well understand the strong spin-lattice correlation between AFM ordering and ZTE behavior. The ZTE in the noncoplanar antiferromagnetic ordered system is attributed to the fierce competition between the nearest AFM direct exchange and ferromagnetic superexchange interaction, which is effectively tuned by C occupation. Our work not only paves the way toward understanding the physical origin of ZTE, but it also provides a feasible strategy for the ZTE design, which is also of great significance for promoting the study of a strong correlation system.

DOI: [10.1103/PhysRevB.107.094412](https://doi.org/10.1103/PhysRevB.107.094412)

### I. INTRODUCTION

Thermo-mechanical stability is a critical challenge for functional devices and engineering applications, such as in the aerospace field [1]. Zero thermal expansion (ZTE) materials are promising candidates to prevent functional degeneration caused by thermal stress and size mismatch [2,3]. However, the exploration of ZTE is a recognized challenge. To date, only a few materials with ZTE behavior have been reported in anomalous thermal expansion materials, especially metallic magnetic ZTE compounds, such as Fe-Ni Invar alloys, YbGaGe,  $\text{Mn}_{1-x}\text{Co}_x\text{B}$ ,  $\text{Mn}_{1-x}\text{Ni}_x\text{CoSi}$ ,  $\text{La}(\text{Fe}, \text{Si})_{13}$ ,  $\text{Tb}(\text{Fe}, \text{Co})_2$ ,  $R_2(\text{Fe}, \text{Co})_{17}$  ( $R$  = rare earth), and Mn-based antiperovskite compounds [3–11]. Although the ZTE mechanisms of these materials are generally attributed to the magnetovolume effect (MVE) and spontaneous magnetostriction, the spin-lattice correlation behind is not that clear and should be unified

[12,13]. Among these, the Mn-based antiperovskite  $\text{Mn}_3\text{AX}$  ( $A$  = metal elements,  $X$  = C or N) exhibits not only attractive negative and zero thermal expansion (NTE/ZTE) behavior driven by magnetism, but also abundant magnetic responses in multiple external fields [11,14–18], which make  $\text{Mn}_3\text{AX}$  one of the most fascinating ZTE materials.  $\text{Mn}_3\text{AX}$  compounds have abundant magnetic orderings [19], which are brought about by various magnetic interactions and strong three-dimensional geometric frustration [20,21]. Until now, the ZTE behavior of  $\text{Mn}_3\text{AX}$  was generally attributed to the specific noncollinear  $\Gamma^{5g}$  antiferromagnetic (AFM) ordering [22,23], for example, in  $\text{Mn}_3\text{Cu}_{0.5}\text{Ge}_{0.5}\text{N}$  and  $\text{Mn}_3\text{GaN}$  [24,25]. However, many reports have demonstrated that conventional  $\Gamma^{5g}$  AFM structure can hardly be stable under extreme low temperature to produce wide-range ZTE [18,25,26]. The mechanisms of ZTE in such a strong correlation system are still unclear, and the role of magnetic interaction in spin-lattice coupling is less discussed with direct experimental observation. There is an urgent need for a more efficient physical system with ZTE to be implemented by an effective magnetic structure manipulation strategy.

\*sunying@buaa.edu.cn

†congwang@buaa.edu.cn

The magnetic interaction competition in  $\text{Mn}_3\text{AX}$  is mainly contributed by the nearest-neighbor part within the  $\text{Mn}_6\text{X}$  octahedral, i.e., Mn-Mn direct exchange and right-angled Mn-X-Mn superexchange interaction. Recently, Mochizuki and Kobayashi presented an isotropic spin model in an antiperovskite lattice, and they discussed the magnetic interaction competition theoretically [27,28]. According to the magnetic theory and the Kanamori-Goodenough rule, Mn-Mn is antiferromagnetic ( $J_{\text{AFM}} > 0$ ) while the Mn-X-Mn interaction is ferromagnetic ( $J_{\text{FM}} < 0$ ), respectively [29,30]. The two interactions corresponding to the orbital electron transfer via the path  $t_{2g} - t_{2g}$  and  $e_g - t_{2g}$ , respectively. Additionally, the electron transferring integrals have different exponential dependencies on the interaction distance  $r$  and different functional forms for the spatial distribution [28,31–33]. Meanwhile, based on this, we think it is possible to regulate the magnetic interaction and magnetic structure by using a structural variable, such as the bond length and the structural distortion, to produce abnormality in the thermal expansion. Therefore, there is a fertile playground for studying the spin-lattice mechanism of ZTE in strongly correlated system by tuning the magnetic interaction of an Mn-based antiperovskite.

Mn-based antiperovskite carbide is a good candidate for ZTE due to the abundance of nonequilibrated magnetic ground states with small formation energy differences between them [34,35], which is favorable for sensitive magnetism regulation with a single tiny structural variable. Herein, we report the ZTE behavior induced by a noncoplanar AFM ordering in an antiperovskite. We present the tunable thermal expansion behavior by magnetic interaction regulation in carbide  $\text{Mn}_3\text{Zn}_{0.5}\text{Sn}_{0.5}\text{C}_x$ , which is revealed by neutron powder diffraction (NPD) experimentally and Monte Carlo simulation. The occurrence of ZTE is highly correlated with the enhanced competition between FM and AFM exchange interaction. Our present work promotes the further understanding of ZTE in magnetic materials, and we propose a strategy for the rational design of ZTE by magnetic interaction regulation.

## II. EXPERIMENTAL TECHNIQUES

Polycrystalline  $\text{Mn}_3\text{Zn}_{0.5}\text{Sn}_{0.5}\text{C}_x$  ( $x = 0.89, 1.00$ ) samples were synthesized by the solid-phase reaction method under vacuum. Metal powder of Mn, Zn, Sn, and C powder (99.99% purity) were weighted and mixed in the stoichiometric ratio. Here the C concentration was employed in excess of the stoichiometric ratio in the initial mixtures considering the low chemical reactivity of carbon. After full grinding, each mixture was pressed into pellets at 20 MPa and then sealed in a quartz tube in vacuum. Finally, the quartz tubes were annealed at 800 °C for 80 h in the furnace and naturally cooled to room temperature.

The crystal structure, thermal expansion behavior, and magnetic structure of the samples were characterized by *in situ* variable-temperature neutron powder diffraction (NPD) under a monochromatic neutron beam [36]. Rietveld refinement of NPD patterns was conducted using the General Structure Analysis System (GSAS) program [37,38]. The thermal expansion properties were measured by a dilatometer (NETZSCH DIL402C) corrected by a fused silica reference sample. The temperature-dependent and field-dependent

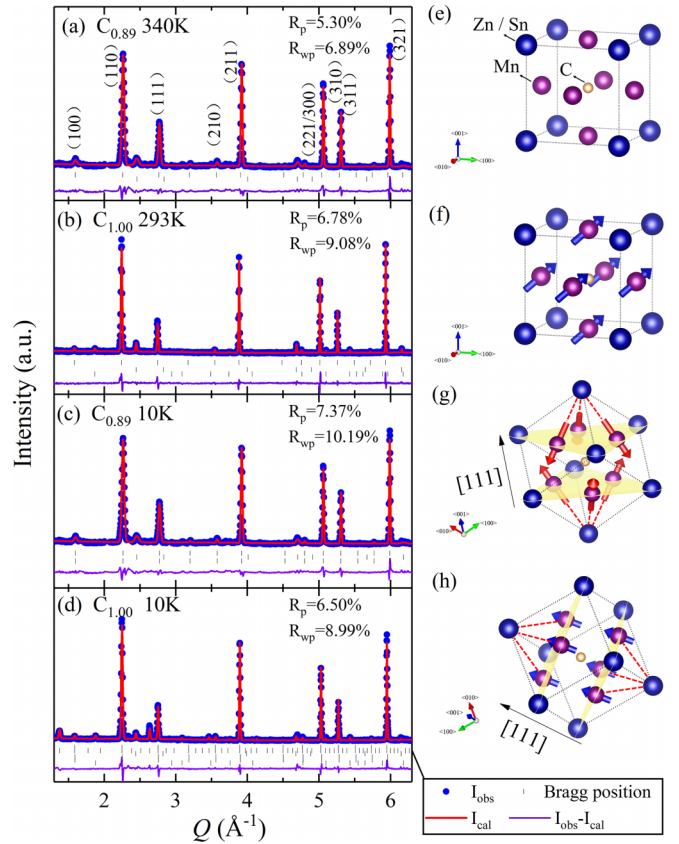


FIG. 1. (a)–(d) NPD patterns of  $\text{C}_{0.89}$  and  $\text{C}_{1.00}$  samples refined with the Rietveld method: (a), (b) Patterns collected in the paramagnetic temperature range (at 340 and 293 K, respectively) and refined with nuclear structure only. (c), (d) Patterns collected at 10 K and refined with nuclear and magnetic structure. (e) The crystal structure of  $\text{Mn}_3\text{Zn}_{0.5}\text{Sn}_{0.5}\text{C}_x$  samples with cubic antiperovskite structure with  $Pm\bar{3}m$  symmetry. (f) Ferromagnetic (FM) structure along (111) orientation with  $P4/mmm'$  symmetry of the  $\text{C}_{0.89}$  sample. (g) Noncoplanar AFM structure with  $R\bar{3}c$  symmetry and propagation  $k = [\frac{1}{2}, \frac{1}{2}, \frac{1}{2}]$  of the  $\text{C}_{1.00}$  sample. (h) Schematic diagram of coexisting FM components in the  $\text{C}_{1.00}$  sample (red dotted line indicates the noncoplanar AFM magnetization direction).

magnetization characteristics are measured using Physical Property Measurement System (PPMS-DynaCool, Quantum Design).

Monte Carlo (MC) simulation was performed on a self-written program using the METROPOLIS algorithm. The system scale was  $12 \times 12 \times 12$  with periodic boundary conditions. The temperature is nondimensionalized as  $k_B T / |J_1|$  in the simulation, ranging from 0 to  $3 k_B T / |J_1|$ . The state (spin alignment and thermal expansion) of each temperature point is iterated independently. We performed 5000 MC sweeps for equilibration, followed by 25 000 MC sweeps for measurement.

## III. RESULTS AND DISCUSSION

The crystal structure of  $\text{Mn}_3\text{Zn}_{0.5}\text{Sn}_{0.5}\text{C}_x$  ( $x = 0.89, 1.00$ ) samples is first examined by NPD combined with Rietveld refinement. Figures 1(a) and 1(b) show the refined NPD patterns of  $\text{Mn}_3\text{Zn}_{0.5}\text{Sn}_{0.5}\text{C}_{0.89}$  and  $\text{Mn}_3\text{Zn}_{0.5}\text{Sn}_{0.5}\text{C}_{1.00}$  at 340

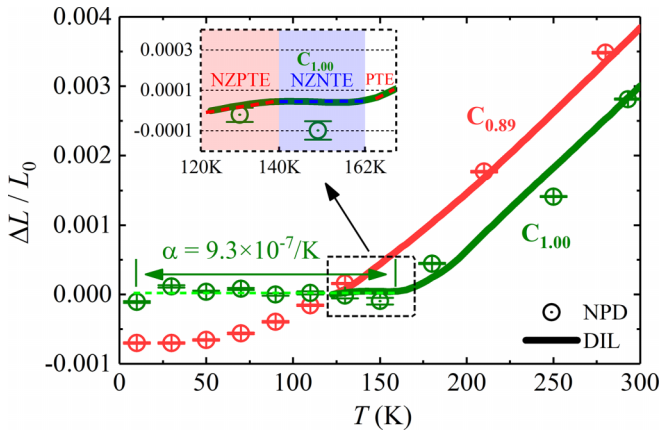


FIG. 2. Thermal expansion of  $C_{0.89}$  and  $C_{1.00}$  samples, where  $\Delta L = L - L_0$ , and  $L_0$  is the lattice constant or the macroscopic sample length (normalized to the value at 123 K). Hollow dots represent results calculated from lattice constant change by NPD refinement, and solid curves represent results from DIL measurement. DIL measurement is conducted in a temperature range from 123 to 300 K and a heating rate of  $5 \text{ K min}^{-1}$ .

and 293 K, respectively. The results reveal the typical antiperovskite structure with  $Pm\bar{3}m$  (no. 221) symmetry of the two samples. Mn, C, and Sn/Zn atoms occupy the face-center, body-center, and corner of the cubic cell, respectively, as shown in Fig. 1(e). The elementary occupation of body-centered C is determined as 0.89 and 1.00, respectively, by NPD refinement. To distinguish for short, two samples are named  $C_{0.89}$  and  $C_{1.00}$ . The saturated C occupation of  $C_{1.00}$  is also revealed by the appearance of a simple substance carbon impurity peak in the NPD pattern. With the increase of carbon occupation, the lattice constant increases from  $3.946\ 83(4)$  to  $3.962\ 08(3)$ , while the lattice symmetry remains the same.

Detailed structural parameters are given in the supplemental material [39].

Then the thermal expansion behavior is analyzed combining the NPD refinement and DIL measurement. The thermal expansion behaviors reflected from the lattice constant change and the DIL data are in quite good agreement, as is shown in Fig. 2. Although the carbon occupation slightly increases with lattice symmetry unchanged, an intriguing change from positive thermal expansion (PTE) behavior to ZTE behavior occurs in the  $\text{Mn}_3\text{Zn}_{0.5}\text{Sn}_{0.5}\text{C}_x$  system. The thermal expansion  $\Delta L/L_0$  of the  $C_{0.89}$  sample continuously increases with temperature, showing conventional PTE behavior within the measurement temperature range. However, the  $C_{1.00}$  sample shows ZTE behavior over a wide temperature range from 10 to 162 K, with the linear thermal expansion coefficient (CTE)  $\alpha$  down to  $9.3 \times 10^{-7} \text{ K}^{-1}$ . Additionally, we find the ZTE behavior of  $C_{1.00}$  is actually separated into a nearly zero PTE section (NZPTE,  $\alpha > 0$ ) behavior below 140 K and a nearly zero NTE section (NZNTE,  $\alpha < 0$ ) during the magnetic transition around 150 K. This can be regarded as typical ZTE behavior caused by MVE, indicating the possible existence of a magnetic transition accompanied by a volume change, which needs to be further examined.

To investigate the role of magnetism in thermal expansion behavior, the magnetization characteristics of the samples are investigated by magnetic measurement. Figure 3 shows temperature-dependent magnetization ( $M$ - $T$ ) curves from 5 to 350 K under a magnetic field of  $H = 100 \text{ Oe}$  with zero-field-cooling (ZFC) and field-cooling (FC) modes (cooling field  $H = 100 \text{ Oe}$ ) and isothermal  $M$ - $H$  curves with the magnetic field  $H$  between  $\pm 9 \text{ T}$ . The  $C_{0.89}$  sample shows a ferromagnetic temperature-dependent characteristic under both modes, as is shown in Fig. 3(a). Upon cooling, the  $C_{0.89}$  sample goes into magnetic ordering from a disordered paramagnetic (PM) state at about 310 K, which is regarded as the Curie temperature ( $T_C$ ). From Fig. 3(b), a hysteresis loop and magnetization

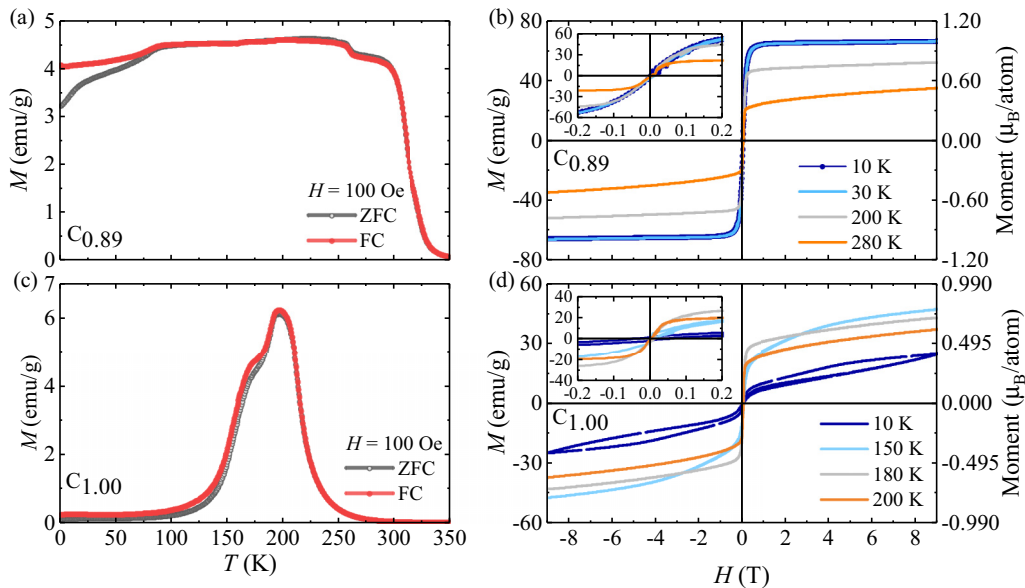


FIG. 3. Temperature-dependent and field-dependent magnetization measurement for samples.  $M$ - $T$  curves under ZFC and FC modes and isothermal  $M$ - $H$  curves of (a), (b)  $C_{0.89}$  and (c), (d)  $C_{1.00}$ .

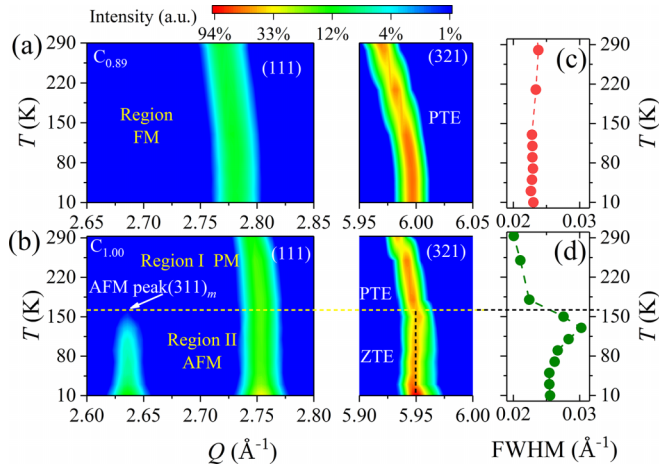


FIG. 4. (a), (b) *In situ* variable-temperature NPD patterns of  $C_{0.89}$  and  $C_{1.00}$  samples showing the (111) and (321) structural reflection and (311)<sub>m</sub> AFM reflection. (c), (d) Peak width (FWHM) change with temperature of the (321) peak at high  $Q$ .

saturation appear in the  $M$ - $H$  curves at 10, 30, 200, and 280 K, respectively, revealing the FM ground state of  $C_{0.89}$ . On the contrary, for the  $C_{1.00}$  sample, the  $M$ - $T$  curves exhibit low magnetization at low temperature, shown in Fig. 3(c), indicating an AFM ground state of  $C_{1.00}$ . The  $M$ - $H$  curves of  $C_{1.00}$  in Fig. 3(d) show unsaturated magnetization combined with small hysteresis, implying that the AFM state coexists with a possible FM component below the ordering temperature. The  $M$ - $H$  curve at 10 K of  $C_{1.00}$  is more significant in unsaturation and coercivity, indicating an obvious AFM characteristic at low temperature. The  $M$ - $T$  curve of  $C_{1.00}$  first rises at the beginning of magnetic ordering and then drops upon further cooling, revealing the evolution of the AFM-FM competition with temperature. There are steplike distortions in  $M$ - $T$  curves around 260 K for  $C_{0.89}$  and around 180 K for  $C_{1.00}$ , which can be attributed to the contribution of short-range magnetism [40]. This can be supported by the fact that the steps of  $C_{0.89}$  and  $C_{1.00}$  are both suppressed when applying a larger field  $H$  (see Fig. S1 of the supplemental material). In Mn-based antiperovskite compounds, considering the spin-lattice correlation, the significant change in thermal expansion behavior can be largely correlated to the long-range magnetic ordering from FM to AFM. Therefore, the long-range magnetic order needs to be further determined by NPD analysis.

Further the magnetic structures of  $C_{0.89}$  and  $C_{1.00}$  is investigated by *in situ* NPD analysis. The magnetic ground state is solved to change from FM in  $C_{0.89}$  to AFM in  $C_{1.00}$  with increasing C occupation. To be specific, for  $C_{0.89}$ , the absence of AFM peaks in the pattern confirms that the ground state of  $C_{0.89}$  is FM, as shown in Fig. 4(a). According to the refinement result [see Fig. 1(c)], the FM structure corresponds to the  $P4/mmm'$  (no. 123.345) magnetic space group with magnetization along the (111) orientation, as the diagram in Fig. 1(f) shows. For the  $C_{1.00}$  sample, the magnetic ordering below around 150 K is accompanied by the appearance of AFM peaks in NPD patterns, illustrated by the (311)<sub>m</sub> peak change with temperature in Fig. 4(b) and the refinement result in Fig. 1(d). The magnetic ordering of the  $C_{1.00}$  sample

is determined as a noncollinear AFM structure ( $R\bar{3}c$  symmetry, no. 167.108 magnetic space group) with noncoplanar magnetization and propagation vector  $k = [\frac{1}{2}, \frac{1}{2}, \frac{1}{2}]$ , called noncoplanar  $[\frac{1}{2}, \frac{1}{2}, \frac{1}{2}]$  AFM for short. The spin alignment of noncoplanar  $[\frac{1}{2}, \frac{1}{2}, \frac{1}{2}]$  AFM is shown in Fig. 1(g). It should be mentioned that the FM ordering of  $C_{0.89}$  does not produce any abnormality in thermal expansion, while the ZTE temperature range of  $C_{1.00}$  largely coincides with that of the noncoplanar AFM ordering. For the  $C_{1.00}$  sample, the (321) peak at a high  $Q$  value, which is considered to be a purely nuclear peak, has a consistently significant width broadening in the AFM ordered region, as the significantly increased FWHM of (321) peak shows in Fig. 4(d). This is different from the case for  $C_{0.89}$  in Fig. 4(c), which reveals another phase coexisting with noncoplanar  $[\frac{1}{2}, \frac{1}{2}, \frac{1}{2}]$  AFM in  $C_{1.00}$ . According to the additional intensity observed on top of the nuclear peaks of the patterns below 180 K, the coexisting phase is determined to be FM ordered. The FM structure has  $P4/mmm'$  symmetry, as Fig. 1(h) illustrates. It is worth mentioning that the ZTE behavior within noncoplanar  $[\frac{1}{2}, \frac{1}{2}, \frac{1}{2}]$  AFM ordering was first reported in magnetic functional materials, exhibiting a different case from the  $\Gamma^{5g}$ -type AFM system; the lattice-spin correlation in this case has yet to be examined.

To clarify the intrinsic correlation between ZTE behavior and noncoplanar  $[\frac{1}{2}, \frac{1}{2}, \frac{1}{2}]$  AFM ordering, the lattice and magnetism evolution of the  $C_{1.00}$  sample with temperature is analyzed according to dual-phase Rietveld refinement. Such refinement strategy is conducted considering that the two magnetic orderings (AFM phase and FM phase) coexist through two structural phases with the same lattice symmetry but different volume, which can be crucial for producing ZTE. As the results show in Fig. 5, from the PM state with a decrease of temperature, the FM component first appears around 180 K with a magnetic moment  $m_{FM}$  of  $0.421\mu_B/\text{at}$ . When a decrease to 150 K noncoplanar  $[\frac{1}{2}, \frac{1}{2}, \frac{1}{2}]$  AFM ordering appears ( $m_{AFM} = 1.340\mu_B/\text{at}$ ). Both the AFM moment and the coexisting FM moment increase with decreasing temperature. Additionally, the coexisting FM moment of  $C_{1.00}$  is smaller than that of  $C_{0.89}$ , which is also consistent with the smaller field-dependent magnetization of  $C_{1.00}$  than  $C_{0.89}$ , indicating the weakened FM interaction and ground-state change from FM to AFM with increasing carbon occupation  $x$ . The fraction of two phases is also temperature-dependent. The two magnetic phases first coexist most remarkably upon the appearance of AFM ordering around 150 K, where the FM phase fraction reaches a maximum of 60.6%. Then the fraction of the AFM phase becomes larger with decreasing temperature and exceeds 83% from 110 to 10 K, resulting in AFM domination. Corresponding to the temperature-dependent magnetization of  $C_{1.00}$ , the increase of magnetization at 250 K is consistent with the earlier formation of FM ordering than noncoplanar AFM, and the decrease at 150 K is consistent with the rapid increase of antiferromagnetic phase content. The noncoplanar  $[\frac{1}{2}, \frac{1}{2}, \frac{1}{2}]$  AFM phase and FM phase have different lattice constants upon phase separation. The most interesting is that the lattice constant of the AFM phase remains unchanged with temperature below ordering temperature, while the FM lattice shows a continuous expansion with temperature within the measured temperature range. Considering the combined

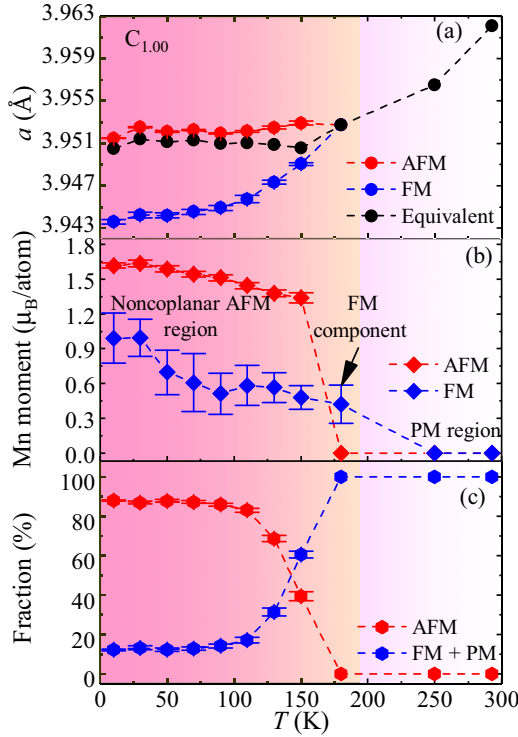


FIG. 5. Lattice, phase, and magnetic moment evolution of the  $C_{1.00}$  sample, revealed by *in situ* NPD refinement: (a) lattice constant  $a$ , (b) Mn magnetic moment, and (c) phase fraction change with temperature. The dual-phase Rietveld refinement is done with two coexisting structural phases with the same lattice symmetry but different magnetic orderings; the magnetic phase fraction is dependent on the structural phase fraction.

contribution of the two, the equivalent lattice constant  $a_{\text{equ}}$  also barely changes with temperature ( $a_{\text{equ}} = a_1 \times F_1 + a_2 \times F_2$ , where  $a_1, a_2$  are the lattice constants, and  $F_1, F_2$  are the fractions of the AFM and FM phases, respectively). Therefore, from the microscopic lattice scale, ZTE is purely a contribution of the AFM phase.

For the ZTE compound  $C_{1.00}$ , the analyses by macroscopic magnetic measurement and *in situ* NPD characterization are in quite good agreement, jointly revealing the noncoplanar AFM ground state and the magnetism evolution of  $C_{1.00}$ . Although there is AFM-FM interaction competition and phase separation in the system, the ZTE behavior of noncoplanar AFM phase is clarified. We can further conclude that the ZTE behavior of  $C_{1.00}$  below 162 K is induced by noncoplanar  $[\frac{1}{2}, \frac{1}{2}, \frac{1}{2}]$  AFM ordering according to the thermal expansion measurement and magnetic analysis above. Such a stable Mn magnetic moment in AFM phase is beneficial to exhibiting ZTE by our previous study in the  $\Gamma^{5g}$  system [11,14]. In the noncoplanar AFM dominant temperature range, the AFM ordered moment decreases gradually with temperature below ordering temperature. Therefore, noncoplanar antiferromagnetic systems exhibit similar spin-lattice correlations, which forcefully clarifies the intrinsic nature of ZTE behavior induced by noncoplanar  $[\frac{1}{2}, \frac{1}{2}, \frac{1}{2}]$  antiferromagnetism.

To numerically investigate the occurrence of ZTE in a Mn-based antiperovskite system, the evolution of thermal ex-

pansion behavior with magnetic interaction is investigated by Monte Carlo simulation. We adapt the spin model, which was first proposed by Mochizuki *et al.* in Refs. [27,28], to describe our system with noncoplanar  $[\frac{1}{2}, \frac{1}{2}, \frac{1}{2}]$  AFM ordering. In a antiperovskite lattice, the magnetism of the system originates from the face-centered Mn atoms. The spin Hamiltonian for the system is written as

$$H = H^{\text{HE}} + H^{\text{MA}} + H^{\text{EP}}, \quad (1)$$

with

$$H^{\text{HE}} = \sum_{i,j} J_{ij} \langle S_i, S_j \rangle,$$

$$H^{\text{MA}} = \sum_i J_{\text{MA}} \langle S_i, e_n \rangle^2, \quad (2)$$

$$H^{\text{EP}} = k_1 \delta^2 - k_2 \delta^3,$$

where  $H^{\text{HE}}$ ,  $H^{\text{MA}}$ , and  $H^{\text{EP}}$  represent energies from the Heisenberg exchange interaction, the magnetic anisotropy, and the phonon, respectively;  $S_i$  is the Mn spin vector in three dimensions and with a fixed length ( $|S_i| = 1$ );  $J_{ij}$  is the Heisenberg exchange coupling;  $J_{\text{MA}}$  is the magnetic anisotropy;  $e_n$  is a directional unit vector pointing vertically out of the cubic surface;  $k$  is the elastic coefficient of the phonon, and  $\delta$  is the thermal expansion of the lattice;  $k_1 \delta^2$  and  $k_2 \delta^3$  represent the harmonic and anharmonic contributions of phonon vibration, respectively.

Here, only the nearest-neighbor coupling  $J_1$  and next-nearest-neighbor coupling  $J_2$  are considered, as demonstrated in Fig. 6(a). Since the nearest Mn-Mn direct exchange interaction (antiferromagnetic,  $J_{\text{AFM}} > 0$ ) and Mn-C-Mn superexchange interaction (ferromagnetic,  $J_{\text{FM}} < 0$ ) have a different dependence on interaction distance  $r$ , which is affected by lattice thermal expansion,  $J_{\text{AFM}}$  and  $J_{\text{FM}}$  depend differently on  $\delta$ . Thus, the nearest-neighbor exchange integral  $J_1$  is written as a function of  $\delta$  as  $J_1(\delta) = J_{\text{AFM}}(\delta) - |J_{\text{FM}}(\delta)|$ . We regulate the relative ratio of the exchange integral between AFM-typed Mn-Mn interaction and FM-typed Mn-C-Mn interaction within the  $\text{Mn}_6\text{C}$  octahedral. During the simulation, the spin alignment of Mn atoms is initialized as the  $[\frac{1}{2}, \frac{1}{2}, \frac{1}{2}]$  AFM. For the nearest interaction, we vary the ratio of  $|J_{\text{FM}}|/J_{\text{AFM}}$  ( $J_{\text{AFM}}/|J_{\text{FM}}|$ ) for the FM (AFM) dominated system, and meanwhile we fix  $|J_1|$  to 1. The next-nearest-neighbor coupling  $J_2$  is fixed to 1 to produce isotropic  $\frac{1}{2}$  spin propagation. The magnetic anisotropic  $J_{\text{MA}}$  is fixed at  $-2$ . The elastic coefficients  $k_1$  and  $k_2$  are fixed at 100 and 200, respectively.

Figure 6(b) shows the simulated thermal expansion evolution with different ratios between  $J_{\text{FM}}$  and  $J_{\text{AFM}}$ . The magnetic order converges to  $[\frac{1}{2}, \frac{1}{2}, \frac{1}{2}]$  AFM below temperature around  $1.5 k_B T / |J_1|$ , above which the spin alignment becomes disordered (PM). The occurrence of AFM-PM magnetic transition can be revealed by sharp peak in specific heat  $C_H$  and a fast change of spin correlation  $\hat{S}$  (see Fig. S5 [39]). The thermal expansion  $\delta$  decreases rapidly during the magnetic transition, shown in Fig. 6(b), which can be regarded as MVE. The systems exhibit PTE in a PM state above the transition temperature, while the change of thermal expansion

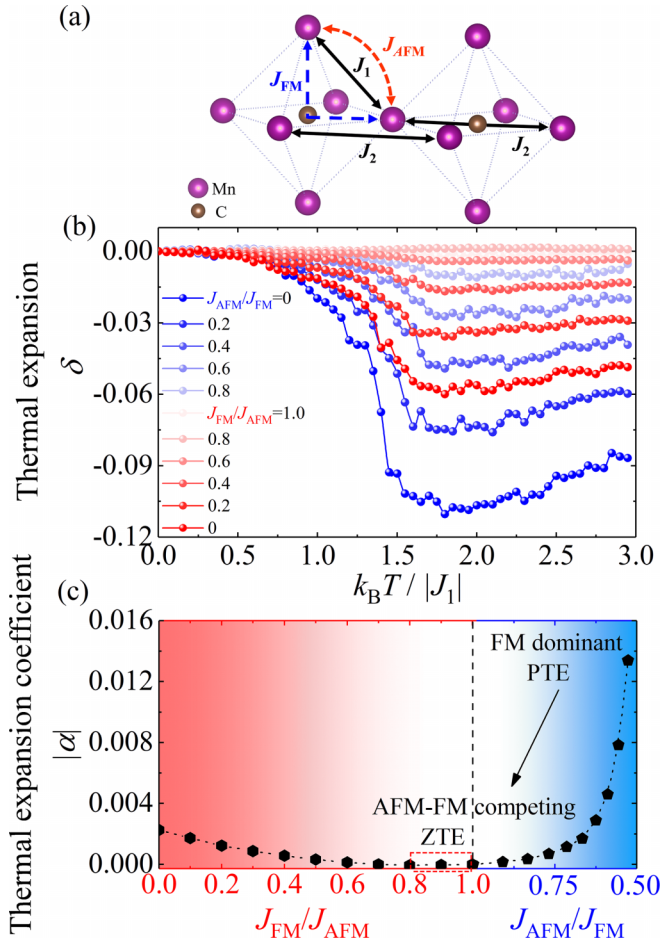


FIG. 6. (a) Schematic demonstration of the Heisenberg interactions between Mn atoms.  $J_1$  is composed of  $J_{AFM}$  and  $J_{FM}$ . (b) Thermal expansion evolution with different ratios between  $J_{FM}$  and  $J_{AFM}$ , obtained from Monte Carlo simulation. (c) Thermal expansion coefficient  $|\alpha| = \left| \frac{d\delta}{dT} \right| (T_u = k_B T / |J_1|)$  in the magnetic ordering temperature range with a different ratio between  $J_{FM}$  and  $J_{AFM}$ .

$\delta$  is relatively low below the transition temperature, attributed to a lower phonon anharmonic contribution and slower spin correlation evolution with temperature in a magnetic ordered state. Obviously, the thermal expansion behavior is largely related to magnetic interaction. Figure 6(c) shows the change of thermal expansion coefficient  $|\alpha|$  in the magnetic ordered state with different magnetic interaction. With the enhancement of  $J_{FM}$ , the thermal expansion within  $[\frac{1}{2}, \frac{1}{2}, \frac{1}{2}]$  AFM ordering temperature is first suppressed in AFM dominant ( $|J_{FM}|/J_{AFM} < 1$ ) systems, and then it recovers and increases rapidly in the FM dominant system ( $J_{AFM}/|J_{FM}| < 1$ ). When  $J_{FM}$  is competitive with  $J_{AFM}$  ( $0.8 < |J_{FM}|/J_{AFM} < 1.0$ ),  $|\alpha|$  reaches a negligible extent, especially compared with that in the FM dominant PTE region. The change of thermal expansion behavior caused by MVE also becomes indistinctive when FM and AFM interactions compete fiercely with each other. Therefore, the fierce FM-AFM competition results in the occurrence of ZTE in the noncoplanar AFM ordered system.

Accordingly, we could well demonstrate the origin of ZTE behavior induced by noncoplanar  $[\frac{1}{2}, \frac{1}{2}, \frac{1}{2}]$  AFM or-

dering with enhanced magnetic interaction competition in  $Mn_3Zn_{0.5}Sn_{0.5}C_x$ . First, with increasing carbon concentration, the lattice volume increases significantly due to the filling of the C site, which will directly increase the magnetic interaction distance of nearest Mn-Mn and Mn-C-Mn. It should be noted that the initial state of the magnetic interaction is determined by carbon occupation, because the interaction distance change caused by different carbon occupation ( $\sim 10^{-3}$ ) is much more significant than that caused by cumulative thermal expansion ( $\sim 10^{-5}$  from 10 to 150 K). Since the nearest Mn-Mn AFM interaction and the Mn-C-Mn FM interaction have different dependences on interaction distance,  $|J_{FM}|/J_{AFM}$  tends to be smaller with a larger C concentration. Second, an increase in carbon occupation introduces possible tensile strain to the  $Mn_6C$  octahedral, and it leads to coordination distortion [41]. Although the bonding density between Mn and C increases, the Mn-C-Mn superexchange interaction is largely weakened, also causing smaller  $|J_{FM}|/J_{AFM}$ . Therefore, the magnetic interaction of the system changes from FM dominant to AFM-FM competing as the arrow shows in Fig. 6(c), which is consistent with the experimental magnetic structure characterization. Both the thermal expansion below ordering temperature and the MVE during the magnetic transition are significantly suppressed, which is consistent with the experimental NZPTE and NZNTE behavior. The system shows ZTE over a wide temperature range consequently. The experimental results combined with the numerical calculation have good uniformity in the explanation of ZTE, revealing that ZTE behavior is induced by the fierce FM-AFM interaction competition in a noncoplanar AFM ordered system. This result can be a practical experimental extension of the spin model by a noncoplanar non- $\Gamma^{5g}$  AFM situation.

In an antiperovskite carbide system with itinerant-electron behavior, the magnetic ordering is largely correlated to the electronic structure. The unusual thermal expansion change from PTE to ZTE induced by noncoplanar magnetization and FM-AFM competition can be fundamentally attributed to the electromagnetic properties tuned by C concentration. Hybridization exists between Mn 3d and C 2p orbits, and the Mn 3d band dominates in the system [21]. An increase of C occupation broadens the degenerated  $d^3$  state of Mn [42], and it directly affects the initial density of states near the Fermi level, enhancing the valence electron transfer during the magnetic transition, and determining the magnetic interaction competition and the stability of the magnetic ground state [43,44]. Meanwhile, the system is free from crystal-field symmetry change and a local cluster, which is mainly determined by the A site. This conclusion can be extended to other magnetic systems.

#### IV. CONCLUSION

In summary, wide-range ZTE behavior is induced by noncoplanar AFM in an antiperovskite  $Mn_3Zn_{0.5}Sn_{0.5}C_x$  system as a practical example of directly regulating the magnetic interaction integral  $|J_{FM}|/J_{AFM}$ . An effective regulation of thermal expansion behavior from conventional PTE to ZTE is achieved by tuning the magnetic ground state from FM to AFM in the antiperovskite system  $Mn_3Zn_{0.5}Sn_{0.5}C_x$ .

ZTE behavior is first proved to be strongly correlated with noncoplanar  $[\frac{1}{2}, \frac{1}{2}, \frac{1}{2}]$  AFM ordering in antiperovskite compounds. This breaks the universal viewpoint in antiperovskite compounds since ZTE always occurs in  $\Gamma^{5g}$  AFM phase in the current reports. In combination with numerical calculations using the spin model, the magnetic interaction competition in a noncoplanar AFM ordered system is quantified within  $0.8 < |J_{FM}|/J_{AFM} < 1.0$  to produce ZTE behavior. Our results provide a strategy for producing ZTE by magnetic structure design, which is significant to revealing the physical nature of strong electro-magneto-lattice correlated systems.

## ACKNOWLEDGMENTS

This work was supported by the National Natural Science Foundation of China (NSFC) (Grants No. 51972013, No. 51732001, No. 52272264, and No. U1832219), and Chinese-German Mobility Programme Project No. M-0273. We appreciate the support by Peking University High Intensity Powder Diffractometer (PKU-HIPD) at China Institute of Atomic Energy (CIAE), and Key Laboratory of Neutron Physics and Institute of Nuclear Physics and Chemistry, China Academy of Engineering Physics during the neutron powder diffraction measurement.

- 
- [1] Y. Zhang, B. Chen, D. Guan, M. Xu, R. Ran, M. Ni, W. Zhou, R. O'Hayre, and Z. Shao, Thermal-expansion offset for high-performance fuel cell cathodes, *Nature (London)* **591**, 246 (2021).
- [2] A. Sleight, Zero-expansion plan, *Nature (London)* **425**, 674 (2003).
- [3] J. R. Salvador, G. Fu, T. Hogan, and M. G. Kanatzidis, Zero thermal expansion in YbGaGe due to an electronic valence transition, *Nature (London)* **425**, 702 (2003).
- [4] P. Mohn, A century of zero expansion, *Nature (London)* **400**, 18 (1999).
- [5] H. Wada and M. Shiga, Thermal expansion anomaly and Invar effect of  $Mn_{1-x}Co_xB$ , *J. Magn. Magn. Mater.* **104–107**, 1925 (1992).
- [6] J. Liu, B. Ding, Y. Yao, X. Xi, Z. Cheng, J. Wang, C.-w. Wang, G. Wu, and W. Wang, Coherent spin rotation-induced zero thermal expansion in MnCoSi-based spiral magnets, *NPG Asia Mater.* **13**, 70 (2021).
- [7] S. Li, R. Huang, Y. Zhao, W. Wang, Y. Han, and L. Li, Zero thermal expansion achieved by an electrolytic hydriding method in  $La(Fe, Si)_{13}$  compounds, *Adv. Funct. Mater.* **27**, 1604195 (2017).
- [8] Y. Song, J. Chen, X. Liu, C. Wang, J. Zhang, H. Liu, H. Zhu, L. Hu, K. Lin, S. Zhang, and X. Xing, Zero thermal expansion in magnetic and metallic  $Tb(Co, Fe)_2$  intermetallic compounds, *J. Am. Chem. Soc.* **140**, 602 (2018).
- [9] W. Li, K. Lin, Y. Yan, C. Yu, Y. Cao, X. Chen, C.-w. Wang, Kato K, Y. Chen, K. An *et al.*, A seawater-corrosion-resistant and isotropic Zero Thermal Expansion (Zr, Ta)(Fe, Co)<sub>2</sub> Alloy, *Adv. Mater.* **34**, 2109592 (2022).
- [10] Y. Cao, K. Lin, S. Khmelevskiy, M. Avdeev, K. M. Taddei, Q. Zhang, Q. Huang, Q. Li, K. Kato, C. C. Tang *et al.*, Ultrawide Temperature Range Super-Invar Behavior of  $R_2(Fe, Co)_{17}$  Materials ( $R =$  Rare Earth), *Phys. Rev. Lett.* **127**, 055501 (2021).
- [11] C. Wang, L. Chu, Q. Yao, Y. Sun, M. M. Wu, L. Ding, J. Yan, Y. Na, W. Tang, G. Li, Q. Huang, and J. W. Lynn, Tuning the range, magnitude, and sign of the thermal expansion in intermetallic  $Mn_3(Zn, M)_xN(M = Ag, Ge)$ , *Phys. Rev. B* **85**, 220103(R) (2012).
- [12] Y. Song, N. Shi, S. Deng, X. Xing, and J. Chen, Negative thermal expansion in magnetic materials, *Prog. Mater. Sci.* **121**, 100835 (2021).
- [13] E. Liang, Q. Sun, H. Yuan, J. Wang, G. Zeng, and Q. Gao, Negative thermal expansion: Mechanisms and materials, *Front. Phys.* **16**, 53302 (2021).
- [14] K. Shi, Y. Sun, C. V. Colin, L. Wang, J. Yan, S. H. Deng, H. Lu, W. Zhao, P. Bordet, Y. Kazunari, and C. Wang, Investigation of the spin-lattice coupling in  $Mn_3Ga_{1-x}Sn_xN$  antiperovskites, *Phys. Rev. B* **97**, 054110 (2018).
- [15] B. S. Wang, P. Tong, Y. P. Sun, L. J. Li, W. Tang, W. J. Lu, X. B. Zhu, Z. R. Yang, and W. H. Song, Enhanced giant magnetoresistance in Ni-doped antiperovskite compounds  $GaCMn_{3-x}Ni_x$  ( $x = 0.05, 0.10$ ), *Appl. Phys. Lett.* **95**, 222509 (2009).
- [16] J. Yan, Y. Sun, H. Wu, Q. Huang, C. Wang, Z. Shi, S. Deng, K. Shi, H. Lu, and L. Chu, Phase transitions and magnetocaloric effect in  $Mn_3Cu_{0.89}N_{0.96}$ , *Acta Mater.* **74**, 58 (2014).
- [17] D. Matsunami, A. Fujita, K. Takenaka, and M. Kano, Giant barocaloric effect enhanced by the frustration of the antiferromagnetic phase in  $Mn_3GaN$ , *Nat. Mater.* **14**, 73 (2015).
- [18] K. Shi, Y. Sun, J. Yan, S. Deng, L. Wang, H. Wu, P. Hu, H. Lu, M. Malik, Q. Huang, and C. Wang, Baromagnetic effect in antiperovskite  $Mn_3Ga_{0.95}N_{0.94}$  by neutron powder diffraction analysis, *Adv. Mater.* **28**, 3761 (2016).
- [19] E. F. Bertaut and D. Fruchart, Magnetic studies of the metallic perovskite-type compounds of manganese, *J. Phys. Soc. Jpn.* **44**, 781 (1978).
- [20] D. Tahara, Y. Motome, and M. Imada, Antiferromagnetic Ising model on inverse perovskite lattice, *J. Phys. Soc. Jpn.* **76**, 013708 (2007).
- [21] J. H. Shim, S. K. Kwon, and B. I. Min, Electronic structure of metallic antiperovskite compound  $GaCMn_3$ , *Phys. Rev. B* **66**, 020406(R) (2002).
- [22] K. Takenaka and H. Takagi, Giant negative thermal expansion in Ge-doped anti-perovskite manganese nitrides, *Appl. Phys. Lett.* **87**, 261902 (2005).
- [23] S. Iikubo, K. Kodama, K. Takenaka, H. Takagi, M. Takigawa, and S. Shamoto, Local Lattice Distortion in the Giant Negative Thermal Expansion Material  $Mn_3Cu_{1-x}Ge_xN$ , *Phys. Rev. Lett.* **101**, 205901 (2008).
- [24] X. Song, Z. Sun, Q. Huang, M. Rettenmayr, X. Liu, M. Seyring, G. Li, G. Rao, and F. Yin, Adjustable zero thermal expansion in antiperovskite manganese nitride, *Adv. Mater.* **23**, 4690 (2011).
- [25] K. Takenaka, T. Inagaki, and H. Takagi, Conversion of magnetic structure by slight dopants in geometrically frustrated antiperovskite  $Mn_3GaN$ , *Appl. Phys. Lett.* **95**, 132508 (2009).
- [26] Y. Sun, X. Yuan, X. Tian, S. Zhao, M. Wu, Z. Wang, P. Hu, and C. Wang, Controllable nearly zero thermal expansion behavior in  $Mn_3Zn_{1-x}Cr_xN$  ( $0 \leq x \leq 0.20$ ) compounds, *Scr. Mater.* **162**, 108 (2019).

- [27] M. Mochizuki, M. Kobayashi, R. Okabe, and D. Yamamoto, Spin model for nontrivial types of magnetic order in inverse-perovskite antiferromagnets, *Phys. Rev. B* **97**, 060401(R) (2018).
- [28] M. Kobayashi and M. Mochizuki, Theory of magnetism-driven negative thermal expansion in inverse perovskite antiferromagnets, *Phys. Rev. Mater.* **3**, 024407 (2019).
- [29] J. B. Goodenough, Theory of the Role of Covalence in the Perovskite-Type Manganites [La,  $M(\text{II})$ ]MnO<sub>3</sub>, *Phys. Rev.* **100**, 564 (1955).
- [30] J. Kanamori, Crystal distortion in magnetic compounds, *J. Appl. Phys.* **31**, S14 (1960).
- [31] W. S. Kim, E. O. Chi, J. C. Kim, N. H. Hur, K. W. Lee, and Y. N. Choi, Cracks induced by magnetic ordering in the antiperovskite ZnNMn<sub>3</sub>, *Phys. Rev. B* **68**, 172402 (2003).
- [32] P. Entel, E. Hoffmann, P. Mohn, K. Schwarz, and V. L. Moruzzi, First-principles calculations of the instability leading to the Invar effect, *Phys. Rev. B* **47**, 8706 (1993).
- [33] L. Zhang, B. Wang, Y. Sun, P. Tong, J. Fan, C. Zhang, L. Pi, and Y. Zhang, Critical behavior in the antiperovskite ferromagnet AlCMn<sub>3</sub>, *Phys. Rev. B* **85**, 104419 (2012).
- [34] O. Cakir, F. Cugini, M. Solzi, K. Priolkar, M. Acet, and M. Farle, Dynamics of nonergodic ferromagnetic/antiferromagnetic ordering and magnetocalorics in antiperovskite Mn<sub>3</sub>SnC, *Phys. Rev. B* **96**, 014436 (2017).
- [35] E. T. Dias, K. R. Priolkar, A. K. Nigam, R. Singh, A. Das, and G. Aquilanti, Phase-separated magnetic ground state in Mn<sub>3</sub>Ga<sub>0.45</sub>Sn<sub>0.55</sub>C, *Phys. Rev. B* **95**, 144418 (2017).
- [36] W. Yang, H. Zhao, Y. Lai, G. Qiao, Y. Xia, H. Du, J. Han, C. Wang, S. Liu, Y. Yang, Y. Hou, and J. Yang, Study on the performance of the Neutron Diffractometer (HIPD at CARR) by Monte Carlo simulation and convolution methods, *IEEE Trans. Nucl. Sci.* **65**, 1324 (2018).
- [37] H. M. Rietveld, The rietveld method, *Phys. Scr.* **89**, 098002 (2014).
- [38] B. H. Toby, EXPGUI, a graphical user interface for GSAS, *J. Appl. Crystallogr.* **34**, 210 (2001).
- [39] Supplemental Material at <http://link.aps.org/supplemental/10.1103/PhysRevB.107.094412> for details of Magnetic measurement, Neutron powder diffraction analysis and Monte-Carlo simulation.
- [40] S. Deng, Y. Sun, L. Wang, H. Wu, K. Shi, P. Hu, Q. Huang, and C. Wang, Near-zero temperature coefficient of resistivity associated with magnetic ordering in antiperovskite Mn<sub>3+x</sub>Ni<sub>1-x</sub>N, *Appl. Phys. Lett.* **108**, 041908 (2016).
- [41] P. Lukashev and R. F. Sabirianov, Spin density in frustrated magnets under mechanical stress: Mn-based antiperovskites, *J. Appl. Phys.* **107**, 09E115 (2010).
- [42] P. Tong, B.-S. Wang, and Y.-P. Sun, Mn-based antiperovskite functional materials: Review of research, *Chin. Phys. B* **22**, 067501 (2013).
- [43] B. Y. Qu and B. C. Pan, Nature of the negative thermal expansion in antiperovskite compound Mn<sub>3</sub>ZnN, *J. Appl. Phys.* **108**, 113920 (2010).
- [44] Y. Wen, C. Wang, M. Nie, Y. Sun, L. Chu, and C. Dong, Influence of carbon content on the lattice variation, magnetic and electronic transport properties in Mn<sub>3</sub>SnC<sub>x</sub>, *Appl. Phys. Lett.* **96**, 041903 (2010).